Running title: *Musa* pericarp dehiscence gene

Chromosome-level genome assemblies of *Musa ornata* and *M. velutina* provide insights into pericarp dehiscence and anthocyanin biosynthesis in banana

Tian-Wen Xiao [1,5], Xin Liu [1,5,6], Ning Fu [1,5,6], Tong-Jian Liu [1,5], Zheng-Feng Wang [2,3,5,*], Xue-Jun Ge [4,5], Hui-Run Huang [1,5,*]

[1] Key Laboratory of National Forestry and Grassland Administration on Plant Conservation and Utilization in Southern China, South China Botanical Garden, Chinese Academy of Sciences, Guangzhou 510650, China

[2]Guangdong Provincial Key Laboratory of Applied Botany, South China Botanical Garden, Chinese Academy of Sciences, Guangzhou 510650, China

[3]Key Laboratory of Vegetation Restoration and Management of Degraded Ecosystems, South China Botanical Garden, Chinese Academy of Sciences, Guangzhou, 510650, China

[4]State Key Laboratory of Plant Diversity and Specialty Crops, South China Botanical Garden, Chinese Academy of Sciences, Guangzhou 510650, China

[5]South China National Botanical Garden, Guangzhou 510650, China

[6]University of Chinese Academy of Sciences, Beijing 100049, China

[*]Corresponding authors: Hui-Run Huang, huirun.huang@scbg.ac.cn; Zheng-Feng Wang, wzf@scbg.ac.cn

Email:

Tian-Wen Xiao: xiaotianwen@scbg.ac.cn

Xin Liu: liuxinxin21d@scbg.ac.cn

Ning Fu: funing216@scbg.ac.cn

Tong-Jian Liu: liutongjian@scbg.ac.cn

Zheng-Feng Wang: wzf@scbg.ac.cn

Xue-Jun Ge: xjge@scbg.ac.cn

Hui-Run Huang: huirun.huang@scbg.ac.cn

ORCID:
Tian-Wen Xiao: orcid.org/0000-0002-7479-7089
Xin Liu: orcid.org/0000-0003-4175-9358
Zheng-Feng Wang: orcid.org/0000-0002-7599-7891
Xue-Jun Ge: orcid.org/0000-0002-5008-9475
Hui-Run Huang: orcid.org/0000-0002-4656-5627

Abstract

Musa ornata and *M. velutina* are members of the Musaceae family and are indigenous to the South and Southeast Asia. They are very popular in the horticultural market, but the lack of genomic sequencing data and genetic studies has hampered efforts to improve their ornamental value. In this study, we generated the first chromosome-level genome assemblies for both species by utilizing Oxford Nanopore long reads and Hi-C reads. The genomes of *M. ornata* and *M. velutina* were assembled into 11 pseudochromosomes with genome sizes of 427.85 Mb and 478.10 Mb, respectively. Repetitive sequences comprised 46.70% and 50.91% of the total genomes for *M. ornata* and *M. velutina*, respectively. Differentially expressed gene (DEG) and Gene Ontology (GO) enrichment analyses indicated that upregulated genes in the mature pericarps of *M. velutina* were mainly associated with the saccharide metabolic processes, particularly at the cell wall and extracellular region. Furthermore, we identified polygalacturonase (PG) genes that exhibited higher expression level in mature pericarps of *M. velutina* compared to other tissues, potentially being accountable for pericarp dehiscence. This study also identified genes associated with anthocyanin biosynthesis pathway. Taken together, the chromosomal-level genome assemblies of *M. ornata* and *M. velutina* provide valuable insights into the mechanism of pericarp dehiscence and anthocyanin biosynthesis in banana, which will significantly contribute to future genetic and molecular breeding efforts.

Keywords: banana, ornamental plant, pericarp dehiscence, anthocyanin biosynthesis

Introduction

Banana *(Musa* spp.) comprises approximately 70 herbaceous species, which are distributed in tropical and subtropical regions of Asia and Oceania [1]. This genus is renowned for being one of the most important food crops globally. Current banana cultivars are descendants of pure *M. acuminata* or hybrids of *M. acuminata* and several other *Musa* species [2], but ancestors of some cultivated bananas are still missing [3]. In addition, *Musa* species include many important ornamental species, such as *M. laterita*, *M. ornata*, *M. rosea*, *M. rubra* and *M. velutina* [4,5]. With the rapid development of third-generation sequencing technology, an increasing number of high-quality plant genomes have been assembled and released, which can facilitate crop domestication [6-9], and the advancement of ornamental plants [10-13]. Despite the significance of producing high-quality genomes, there is still a lack of genomic resources for banana cultivars, their wild relatives and ornamental species of *Musa* [but see 14,15-22].

M. ornata W. Roxburgh (Mo) and *M. velutina* H. Wendl. & Drude (Mv) belong to the section *Musa* of the Musaceae family and are closely related to *M. acuminata* [23]. Mo, also referred to as the flowering banana or ornamental banana, is native to Bangladesh, Myanmar and northeast India and is widely cultivated in the tropical countries. It can be identified by its pale lilac-purple bracts with small yellow apices, green peduncles and erect inflorescence (Fig. 1A and 1B) [24]. Mv, commonly known as the pink banana, is native to Myanmar and northeast India and is cultivated in the tropical countries. It can be easily distinguished by its brightly colored pink and hairy fruits that self-peel when mature (Fig. 1D and 1E) [24]. Both Mo and Mv have received the Award of Garden Merit from the Royal Horticultural Society of the United Kingdom. In addition to their ornamental value, their fruits are also a source of food for the local people [25]. These attributes make Mo and Mv desirable candidates for generating high quality genomes to aid future molecular breeding endeavors.

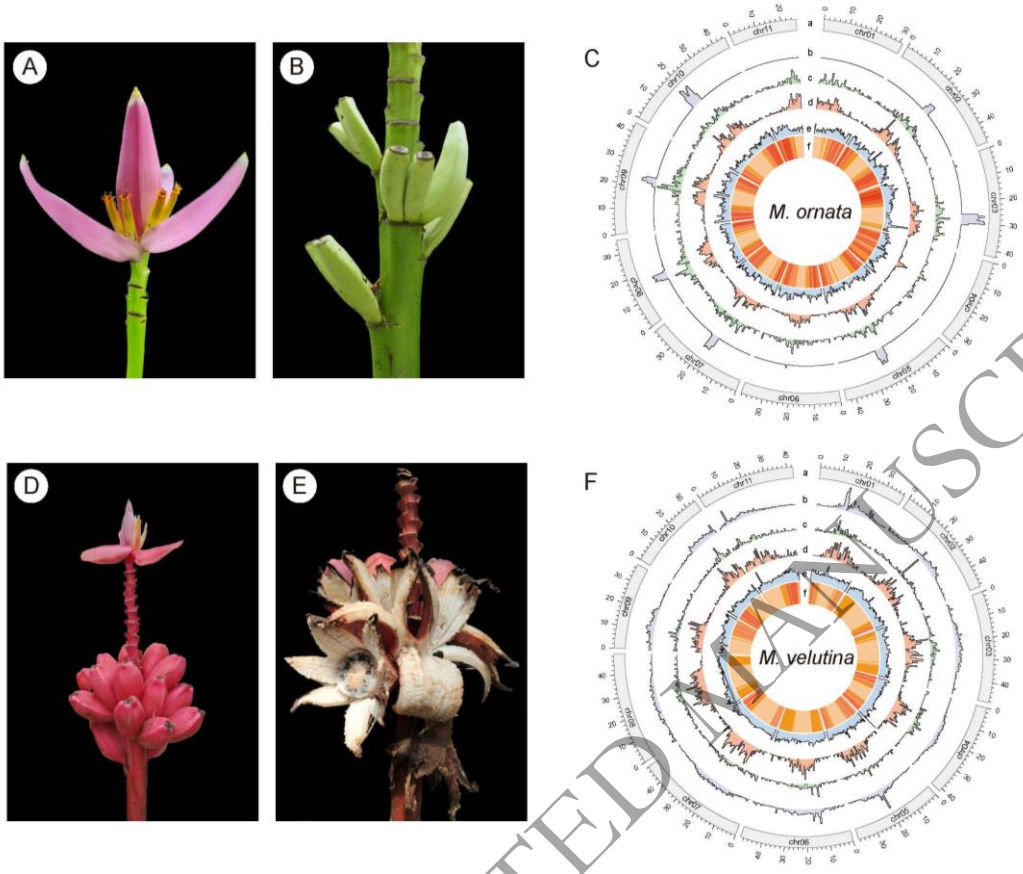

Figure 1 A and **B:** Flowers and fruits of *Musa ornata*. **D** and **E:** Flowers and fruits of *M. velutina*. **C** and **F:** Chromosome characterization of the Mo and Mv genome assemblies, respectively. The tracks from the outer to the inner (a–f) represent the chromosome, tandem repeat density, gypsy element density, copia element density, GC content, and gene density, respectively. These metrics were calculated in 700 kb windows.

Self-peeling (or pericarp-dehiscent) fruits of ornamental plants have the potential to attract more animals than non-self-peeling fruits do, which can be advantageous for the seed dispersal in the wild [26,27] but may cause issues for gardeners. Pericarp dehiscence has been suggested to be correlated with degeneration of the middle lamella [28], which is the outermost layer of cell wall and is rich in pectic polysaccharides [29]. Among many biological functions, the middle lamella plays a crucial role in maintaining the structural integrity of plant tissues and organs by gluing cells together and preventing them from sliding against each other [29]. Polygalacturonase (PG; a pectinase) genes encode enzymes that degrade pectin in

plant cell walls by catalyzing the hydrolysis of α-(1–4) glycosidic bonds in polygalacturonic acid chains, which produces galacturonic acid monomers and oligosaccharides as degradation products [30]. This process is intimately linked to anther dehiscence [31], fruit ripening and cracking [32], and the shedding of leaves, flowers and fruits [33,34]. For example, the overexpression of PG genes promotes cell separation in siliques of *Arabidopsis* and results in pericarp dehiscence [35]. Moreover, the cellulose is the major structural component of the plant cell wall, particularly the primary and secondary cell walls [36]. The cellulase (CEL) genes encode enzymes that degrade cellulose, and they are upregulated during fruit abscission in many plant species [37]. Pericarp dehiscence has been reported in Mv, *M. schizocarpa* and some cultivars of *M. acuminata* [4,38]. However, despite the importance of Mv as an ornamental plant and a close relative of *M. acuminata*, the molecular mechanism of pericarp dehiscence has not been investigated.

Anthocyanins are phenolic compounds that contribute to plant coloration and have important biological functions, including antibacterial effects, removal of excess reactive oxygen species, and attraction to animals for pollination [39,40]. Anthocyanins are synthesized via the phenylpropanoid pathway, which is catalyzed by structural genes such as chalcone synthase (CHS), chalcone isomerase (CHI), flavanone 3-hydroxylase (F3H), dihydroflavonol 4-reductase (DFR), anthocyanidin synthase (ANS) and flavonoid 3-glucosyl transferase (3-GT) [41]. Previous studies have conducted comparative analyses and have indicated that anthocyanins play an important role in the formation of the purple peel of *M. itinerans* [42], as well as the red peel of *Musa* AAA Red green [43]. Although colored bracts and fruits have great ornamental value, the regulation of the anthocyanin biosynthesis pathway in Mo and Mv remains elusive.

To provide additional genomic resources for wild *Musa* species and to explore the molecular mechanism underlying pericarp dehiscence and anthocyanin biosynthesis, we present here the chromosome-scale assemblies of Mo and Mv. These two genomes were constructed using a combination of Nanopore long-read sequencing and Hi-C

scaffolding. Based on genome evolution analyses, we found that Mo and Mv had no species-specific whole genome duplication (WGD) events. The comparative analysis indicated that genome structures were relatively conserved among the two genomes and *M. acuminata*. Differentially expressed gene (DEG) analysis indicated that the upregulated genes in the mature pericarp were involved primarily in saccharide metabolic processes. Furthermore, we identified anthocyanin synthesis-related genes and PG genes that may be responsible for pericarp dehiscence. Our study lays the foundation for genetic analyses of Mo and Mv, provides insights into their genomic features, and provides solid groundwork for future endeavors aimed at crop and ornamental plant improvement.

Results

Genome sequencing and assembly

Table 1 Summary of the genome assemblies of *Musa ornata* and *M. velutina*.

Genome features	***M. ornata***	***M. velutina***
Estimated genome size（Mb)	432.26	464.33
Chromosome number	2n = 2 × 11	2n = 2 × 11
Initial genome assembly size (Mb)	538.58	498.22
Contig Number	259	108
Contig N50 (Mb)	12.88	18.18
Genome size after scaffolding (Mb)	477.18	496.23
Scaffold Number	36	34
Scaffold N50 (Mb)	38.31	42.77
Pseudochromosome length (Mb)	427.85	478.10
Gap numbers	3	6
Telomeres identified	9	8
BUSCO assessment	98.08%	98.51%
LAI	13.68	16.81

The genomes of Mo and Mv were sequenced and assembled in this study. In total, 34.01 Gb and 39.02 Gb of short clean Illumina reads of Mo and Mv were obtained for the genomic survey, respectively (Table S1). According to the 21-mer analysis of the

Illumina reads, the haploid genome size of Mo was estimated to be 432.26 Mb, the heterozygosity was 0.37%, and the repeat content was 40.40% (Fig. S1A). The haploid genome size of Mv was estimated to be 464.33 Mb, the heterozygosity was 0.09%, and the repeat content was 41.10% (Fig. S1B). A total of 57.48 Gb and 56.34 Gb of Nanopore long reads were generated for Mo and Mv, with median read lengths of 18.46 kb and 20.29 kb, and read N50 lengths of 30.57 kb and 30.72 kb, respectively (Table S1). The Nanopore long reads were used for genome assembly. The draft genome size of Mo was 538.58 Mb, consisting of 259 contigs and a contig N50 length of 12.88 Mb. For Mv, the genome size was 498.22 Mb, comprising of 108 contigs with a contig N50 length of 18.18 Mb. The redundant sequences of the draft genomes were then removed, and the genome assemblies were polished using Nanopore and Illumina reads. Subsequently, 235.16 Gb and 271.49 Gb of clean Hi-C reads of Mo and Mv were used for scaffolding, respectively (Table S1). Thereafter, the genome assembly of Mo covered a total of 477.18 Mb and consisted of 36 scaffolds with a scaffold N50 length of 38.31 Mb. In addition, 89.66% of the sequences were anchored to 11 pseudochromosomes, with a cumulative length of 427.85 Mb (Tables 1 and S2). The genome assembly of Mv was 496.23 Mb in length and consisted of 34 scaffolds with a scaffold N50 length of 42.77 Mb; in addition, 96.36% of the sequences (478.10 Mb) were anchored to 11 pseudochromosomes (Tables 1 and S2). The GC ratios of Mo ranged from 35.23% to 46.50%, with an average of 38.62% (Fig. 1C), and Mv ranged from 32.15% to 51.22%, with an average of 38.57% (Fig. 1F). Initially, there were 38 and 37 gaps in the genomes of Mo and Mv, respectively (Table S2). After gap-closing, Mo had three gaps, two on chr01 and one on chr03, whereas Mv had six gaps, one on chr02, one on chr07, and four on chr09 (Fig. S2; Table S2). Nine and eight telomeres were identified in the Mo and Mv genome assemblies, respectively (Fig. S2), with the telomere repeat monomers of Mo and Mv being “AGGCCC” and “AAACCCT”, respectively. The telomeric repeat numbers of Mo ranged from 110 (chr08 right end) to 4,571 (chr05 right end), and those of Mv ranged from 287 (chr06 right end) to 4,277 (chr01 right end) (Table S3). According to the results of the centromere statistical analysis, the

lengths of the potential centromere tandem repeats (TRs) of Mo ranged from 2,917 bp (chr04) to 3,841,662 bp (chr10), and those of Mv ranged from 10,177 bp (chr03) to 742,822 bp (chr02) (Fig. 1C and 1F; Table S4). The location of potential centromeric region was shown in Fig. S2.

The Mo and Mv genomes had high completeness (98.08% and 98.51%, respectively) according to the BUSCO analyses (Fig. S3). A total of 95.55% and 94.29% of the Illumina reads and 97.55% and 98.28% of the RNA reads were mapped to the genomes of Mo and Mv, respectively. The LAIs of Mo and Mv were 13.68 and 16.81, respectively. The Hi-C heatmaps showed that the pseudochromosomes of Mo and Mv were well connected along the diagonal (Fig. S4). Thus, two high-quality chromosome-scale genomes of Mo and Mv were assembled.

Genome annotation

According to the EDTA analysis, 46.70% of the Mo genome was identified as repetitive sequences. Among the major types of TEs identified, long terminal repeats (LTRs) comprised the highest proportion and accounted for 38.97% of the genome; these included 25.86% of *Copia* and 9.76% of *Gypsy* (Table S5). For Mv, ~243 Mb (50.91%) of repetitive sequences were identified, among which LTRs were the major repeats and accounted for 42.75% of the genome. The predominant LTR was *Copia* (30.09%), followed by *Gypsy* (7.18%) (Table S5).

To identify the genes in the Mo and Mv genomes, a combination of *de novo*, transcriptome and homolog-based annotation approaches was applied. Using protein sequences from *Ensete glaucum*, *Musa acuminata*, *M. balbisiana*, *M. itinerans* and *M. schizocarpa* (Table S6) as a homologous database and transcriptome data from leaves, bracts and tepals (Table S1), a total of 39,177 genes encoding 43,848 proteins were predicted with an average gene length of 4,151.19 bp for the Mo genome. Among the protein-coding genes, 35,868 (91.55%) were functionally identified by the EggNOG database, with 27,428 (70.01%), 32,839 (83.82%) and 28,436 (72.58%) of the genes identified by GO, InterProScan and Pfam, respectively (Table S7). Using the same

protein sequences from five species as a homologous database and transcriptome data from leaves, bracts, tepals, pericarps and sarcocarps (Table S1), the Mv genome was found to contain 31,256 genes encoding 36,066 proteins with an average gene length of 4,800.97 bp. Of these protein-coding genes, 31,084 (99.45%) could be identified in the EggNOG database, with 21,768 (69.64%), 25,763 (82.43%) and 25,005 (80.00%) of the genes identified by GO, InterProScan and Pfam, respectively (Table S7). In addition to protein-coding genes, 781 and 990 tRNA genes were annotated in the genomes of Mo and Mv, respectively. According to the BUSCO assessment, the protein sequences of Mo and Mv had completeness score of 95.66% and 87.67%, respectively (Fig. S5).

Phylogeny and gene family expansion and contraction

Protein sequences from Mo, Mv, *M. acuminata*, *M. balbisiana*, *M. beccarii*, *M. itinerans*, *M. schizocarpa*, *M. troglodytarum*, *Ensete glaucum* (Musaceae) and *Wurfbainia villosa* (Zingiberaceae; Table S6) were clustered and grouped into 34,473 gene families. We identified 24,193 gene families in the Mo genome, which was more than those characterized in the genomes of Mv (20,839), *M. balbisiana* (21,567) and *M. troglodytarum* (23,279) but slightly less than the number of gene families in the *M. acuminata* genome (24,606) (Fig. 2A). Moreover, 14,649 gene families were shared by the five *Musa* species, whereas there were 1,052 unique gene families in Mo, which was greater than that in Mv (519) and *M. balbisiana* (397) but less than that in *M. acuminata* (1,479) and *M. troglodytarum* (1,332) (Fig. 2A). We then performed GO enrichment analysis for the unique gene families of Mo and Mv, respectively. The results showed that the unique gene families in Mo were the most significantly enriched in the GO terms “sulfotransferase activity” and “transferase activity, transferring sulphur-containing groups” (Fig. S6A), while the unique gene families in Mv were significantly enriched in the GO terms “disaccharide metabolic process” and “oligosaccharide metabolic process” (Fig. S6B).

To explore the evolutionary relationships of Mo and Mv, we identified 2,641 single-copy gene families among the 10 species and used these genes for phylogenetic tree

reconstruction and divergence time estimation. Our analysis showed that Mo and Mv were sisters and had close relationship with *M. acuminata* (Fig. 2B). Mo and Mv diverged at 6.87 Mya, and they diverged from *M. acuminata* at 8.67 Mya (Figs. 2B and S7). The insertion of *Copia* in *M. acuminata* and Mo peaked at 0.4 Mya and 0.8 Mya, respectively, while Mv peaked at 1.3 Mya, with a second peak occurring at 0.5 Mya (Fig. 2D).

According to the results of gene family expansion and contraction analysis, 834 and 618 gene families of Mo experienced expansion and contraction, respectively (Fig. 2B). Among the expanded gene families, 420 were significant, consisting of 1,717 genes; 181 gene families were significantly contracted with 184 genes (Table S8). For Mv, 370 and 2,943 gene families experienced expansion and contraction, respectively (Fig. 2B). Among the expanded gene families, 124 were significant, consisting of 565 genes; 709 gene families were significantly contracted with 680 genes (Table S8). GO enrichment analysis of the significantly expanded gene families indicated that the genes in Mo were enriched mainly in the GO terms “structural molecule activity”, “structural constituent of ribosome” and “actin binding”. (Fig. S8A), while the Mv expanded genes were enriched in the GO terms “GTPase activity”, “monooxygenase activity” and “chromatin” (Fig. S8B). In contrast, the GO enrichment analysis of the significantly contracted gene families indicated that the genes in Mo were enriched mainly in the GO terms “ATPase-coupled transmembrane transporter activity” and “primary active transmembrane transporter activity” (Fig. S8C), while the Mv contracted genes were enriched in the GO terms “structural molecule activity” and “GTP binding” (Fig. S8D).

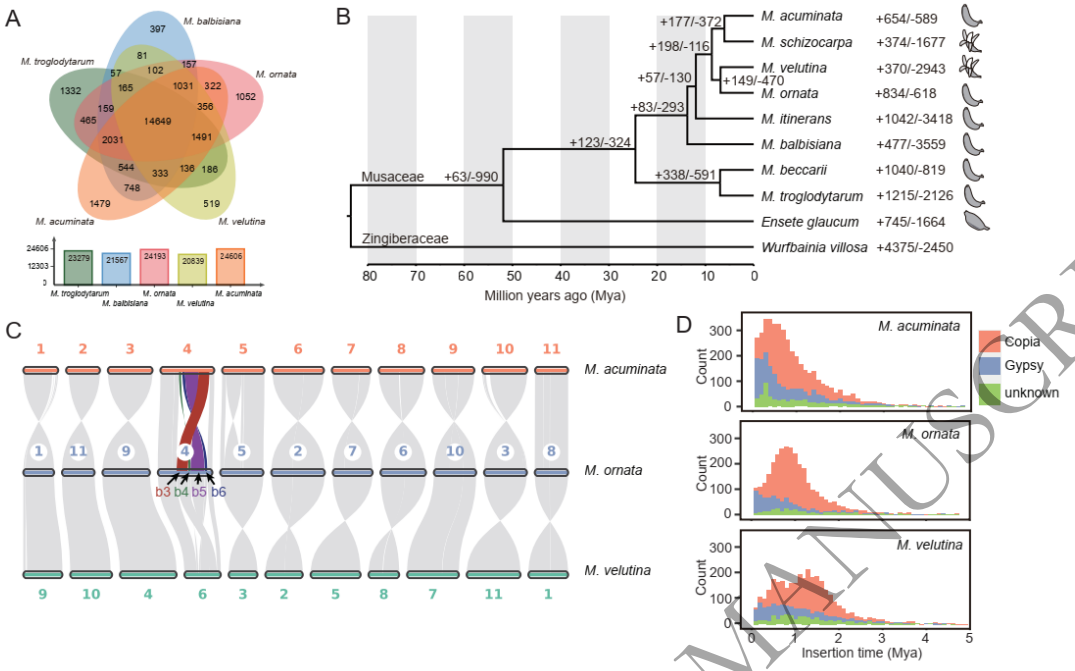

Figure 2 Comparative analysis of gene families between the genomes of Mo, Mv and other species. **A:** The shared and unique gene families among the five genomes of *Musa*. **B:** Divergence time of 10 species based on 2,641 single-copy nuclear genes. The numbers near nodes and species names indicate gene families that have expanded (+) or contracted (-). The fruit sketches indicate the dehiscence or indehiscence of pericarps when mature. **C:** Genome synteny plot. b3, b4, b5 and b6 indicate large blocks with structural variation. **D:** LTR insertion time (bin width = 0.1).

Genome synteny, duplications and whole genome comparisons

A synteny plot showed that the structure of most homologous chromosomes was relatively conserved among Mo, Mv and *M. acuminata*, but inversions and translocations were observed in chr04 of Mo when comparing to Mv and *M. acuminata* (Fig. 2C). Chr04 of Mo can be divided into seven large blocks, among which block 3 was translocated with a size of 6.4 Mb and blocks 4, 5 and 6 were inversed with sizes of 1.6, 9.3 and 2.2 Mb, respectively (Fig. 2C). To ensure that these structural variations were not caused by incorrect assembly, we analyzed the Hi-C signals in the surrounding regions by mapping Hi-C reads to the genome of Mo. Our analysis confirmed the presence of these variations (Fig. S9). Based on the modes of duplication, the Mo genes were classified into WGD, transposed duplication (TRD),

tandem duplication (TD), proximal duplication (PD) and dispersed duplication (DD), containing 12,720, 1,542, 983, 2,146 and 47,164 gene pairs, respectively, and Mv into 8,530, 1,355, 941, 1,449 and 40,033 gene pairs, respectively (Fig. S10; Table S9). After assigning a unique mode of duplication for each gene, 16,245, 1,552, 1,381, 1,031 and 9,195 unique genes of Mo were identified as WGD, TRD, TD, PD and DD, respectively, with 11,860, 1,537, 1,360, 677 and 8,808 unique genes for Mv (Fig. S10; Table S9). The distribution map of synonymous nucleotide substitutions (Ks) (Fig. S11), together with the genome synteny plot showing a collinear pattern of 1:1 (Fig. 2C), suggested that Mo and Mv experienced at least two WGD events. We used *M. acuminata* as a reference to calculate the Ka/Ks of Mo and Mv, and our analysis showed that the two species had similar Ka/Ks distribution patterns (Fig. S12). Furthermore, we selected genes under positive selection (Ka/Ks > 1) for GO enrichment analysis, and the results showed that Mo and Mv were primarily enriched in the GO terms such as "plastid organization", "chloroplast organization" and "defense response" (Fig. S13), suggesting that the two species may have undergone similar selective pressure. The PSMC trajectory showed that Mo and *M. acumianta* had large historical effective population sizes, which began to decrease from ~60,000 years ago to the present. In contrast to those of Mo and *M. acuminata*, Mv had a relatively small historical effective population size (Fig. S14).

Pericarp dehiscence-related genes of Mv

To determine which genes were involved in the pericarp dehiscence of Mv, differentially expressed gene (DEG) analysis was performed. DEGs between different developmental stages of Mv were identified in pericarps (immature pericarps *vs.* mature pericarps, hereafter imPC *vs*. mPC) and sarcocarps (immature sarcocarps *vs.* mature sarcocarps, hereafter imSC *vs*. mSC). In mPC, 3,070 genes were upregulated and 6,871 were downregulated (Table S10). In mSC, 1,967 genes were upregulated and 9,925 were downregulated (Table S11). GO enrichment analysis revealed that the genes upregulated in mPC were enriched in the GO terms "oligosaccharide metabolic process", "disaccharide metabolic process", "extracellular region", "cell wall" and

316 “hydrolase activity, hydrolyzing O-glycosyl compounds” (Fig. 3A; Table S12), while
317 in mSC, the enriched GO terms associated with the upregulated genes were
318 “hydrolase activity, acting on glycosyl bonds” and “hydrolase activity, hydrolyzing O-
319 glycosyl compounds” (Fig. 3B; Table S13). Moreover, the downregulated genes in
320 mPC and mSC were enriched in the GO terms such as “response to endogenous
321 stimulus”, “ribosome” and “structural molecule activity” (Fig. S15).

322 The PG and CEL family genes were detected by searching for protein domains using
323 HMMER v3.3.2 [44]. In total, 38 PG and 28 CEL candidate genes were identified
324 from the protein sequences of Mv after filtering. The PG genes were named MvPG1
325 to MvPG38, and CEL genes were named MvCEL1 to MvCEL28 according to their
326 chromosomal positions (Fig. 3C). Three genes (MvPG11/mv_006393,
327 MvPG6/mv_002398 and MvPG21/mv_18400) that were significantly upregulated
328 according to the DEG analysis (Tables S10 and S11) exhibited higher expression
329 levels in mPC and mSC than in imPC and imSC, bracts, tepals and leaves of Mv,
330 while no PG genes were highly expressed throughout the development stages of the
331 dwarf banana (*Musa* spp. AAA) (Fig. 3D; Table S14). In addition,
332 MvPG7/mv_002400, MvPG10/mv_005824 and MvPG19/mv_015533 were also
333 significantly upregulated (Table S10) and exhibited moderate increases in expression
334 from imPC to mPC (Fig. 3D; Table S14). According to the GO enrichment analysis,
335 MvPG6, MvPG7, MvPG10, MvPG11, MvPG19 and MvPG21 were involved in the
336 molecular functions of “hydrolase activity, hydrolyzing O-glycosyl compounds” and
337 “hydrolase activity, acting on glycosyl bonds” (Tables S12 and S13). The six PG
338 genes were located on chr01, chr04, chr09 and chr11 of the Mv genome (Fig. 3C), and
339 microsynteny analysis revealed that their adjacent regions exhibited good collinearity
340 across different species (Fig. 3F–3J). Among these PG genes, MvPG6 and MvPG7
341 were derived from tandem duplication (TD) (Fig. 3G; Table S9), suggesting that TD
342 may have contributed to the pericarp dehiscence of Mv. In contrast, no CEL genes
343 showed higher expression level in mPC and mSC than in the other tissues (Fig. 3E;
344 Table S14).

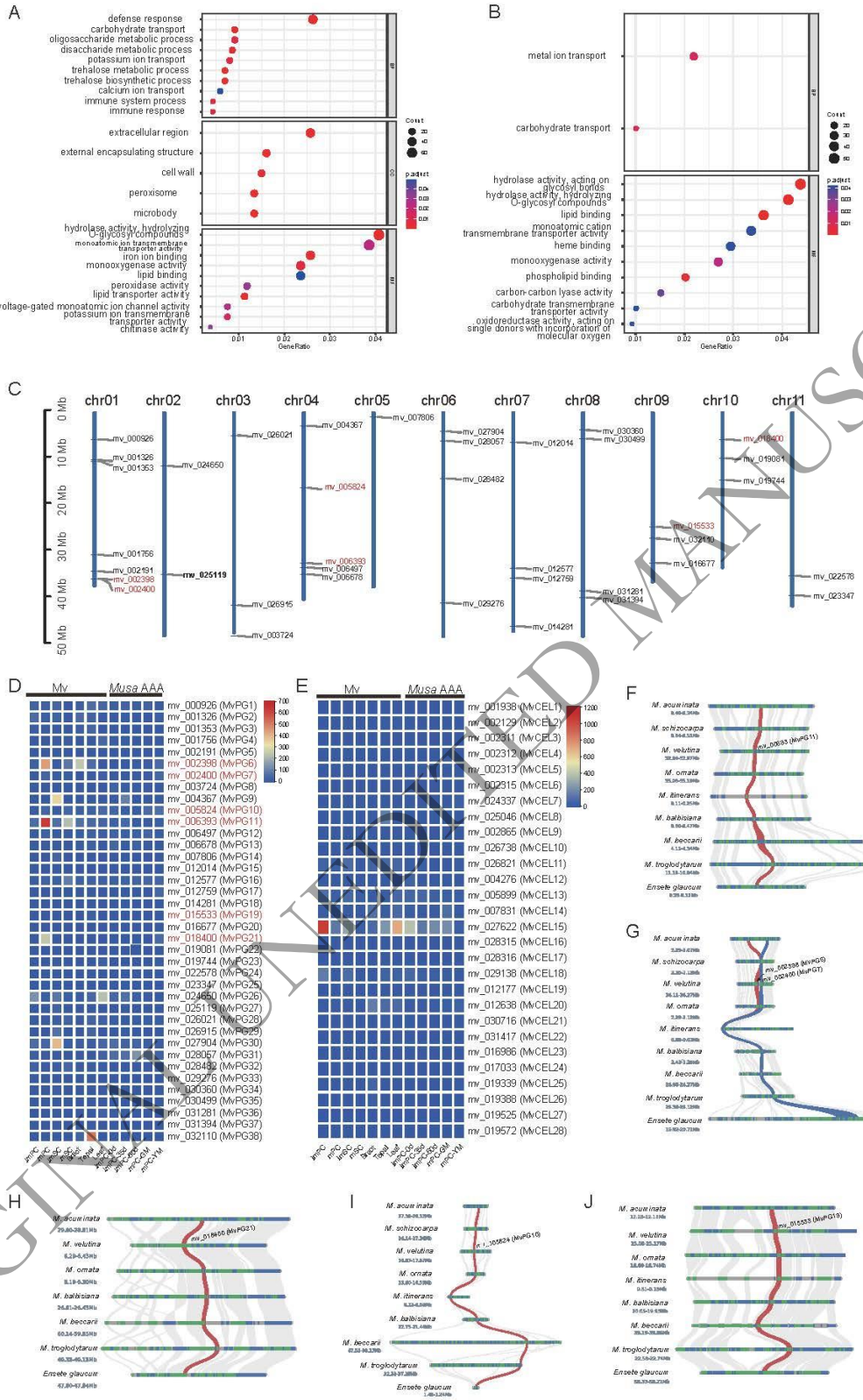

345

346 **Figure 3 A** and **B:** GO enrichment of upregulated genes in pericarps and sarcocarps, respectively.

347 **C:** The location of PG genes on Mv chromosomes. **D:** The expression levels of PG genes in

348 different tissues of Mv and *Musa* spp. AAA. **E:** The expression levels of CEL genes in different

tissues of Mv and *Musa* spp. AAA. **F–J:** Microsynteny of significantly upregulated PG genes across different Musaceae species. BP, biological process; CC, cellular component; MF, molecular function. imPC: immature pericarps; mPC: mature pericarps; imSC: immature sarcocarps; mSC: mature sarcocarps; imPC-0d: immature pericarps from fruits just emerging from the bunch; imPC-35d: immature pericarps from 35-day-old fruits; imPC-60d: immature pericarps from 60-day-old fruits; mPC-GM: mature pericarps from green-matured fruits; mPC-YM: mature pericarps from yellow-matured fruits (6 days after ethylene treatment).

Multiple sequence alignment revealed two variable domains (PGHG and RIK) and two relatively conserved domains (SPNTDG and GDDC) in the PG genes (Fig. S16). The protein sequence divergence of MvPG11/mv_006393 from its orthologs was low, and only one amino acid was uniquely present in MvPG11 (i.e., methionine at position 351 of the alignment). The phylogenetic tree of the PG family showed that orthologs of MvPG11 formed a monophyletic clade (Fig. S17). The Ka and Ks values between gene pairs within the PG family were calculated. The results showed that Ka and Ks were relatively high when MvPG11 was compared to its paralogs (mean Ka = 0.84, mean Ks = 1.92), but Ka and Ks were relatively low when MvPG11 was compared to its orthologs (mean Ka = 0.03, mean Ks = 0.16) (Table S15). Compared to its orthologs, MvPG11 had a mean Ka/Ks of 0.3, suggesting that this gene was under purifying or negative selection and might have a conserved function within the Musaceae and Zingiberaceae.

Previous studies have shown that PG genes can be upregulated by certain transcription factors (TFs), such as AP2/ERF, NAC and MADS-box [45-47]. Therefore, we investigated these TFs in the Mv genome. After filtering, 444 AP2/ERF genes of Mv were obtained, among which 41 genes were upregulated in the mPC, and one gene (mv_002944) exhibited a sharply increased expression level from imPC to mPC (Fig. S18A). We identified 146 NAC genes in Mv, among which 30 genes were upregulated in the mPC, and the expression levels of three genes (mv_002857, mv_025663 and mv_030006) sharply increased from imPC to mPC (Fig. S18B). Furthermore, 73 MADS-box genes in Mv were detected, among which five genes

were upregulated in the mPC, and the expression level of one gene (mv_023703) sharply increased from imPC to mPC (Fig. S18C). To determine whether AP2/ERF, NAC and MADS-box might regulate PG genes and to facilitate future studies, we identified potential transcription factor binding sites (TFBSs) in the upstream regions of the PG genes identified above. For example, 156, 18 and 6 potential TFBSs of AP2/ERF, NAC and MADS-box were predicted for MvPG11; for MvPG6, we predicted 13, 38 and 32 TFBSs for AP2/ERF, NAC and MADS-box, respectively; and for MvPG21, there were 6, 94 and 60 TFBSs for AP2/ERF, NAC and MADS-box, respectively (Table S16).

Anthocyanin biosynthesis pathway

To facilitate horticultural breeding, we investigated the anthocyanin synthesis pathway as well as its upstream phenylpropanoid and flavonoid biosynthesis pathways (Fig. 4A). The number of genes encoding enzymes at each step was retrieved from functional annotations. The C4H gene numbers of Mo and Mv were ten and nine, respectively, which were slightly greater than those of the other species ranging from six to eight. The other structural gene numbers of Mo and Mv were similar to those of the other Musaceae species and *Wufbainia villos*a (Fig. 4B). According to the expression level analysis, several genes such as ANS_1, F3’5’H_7, F3H_2, CHS_9, 4CL_13 and PAL_4 had higher expression levels in immature pericarps (imPC-0d) than in mature pericarps (mPC-GM) of *Musa* spp. AAA (Fig. 4C; Table S17); as for Mv, ANS_1, F3’5’H_7, F3H_2, CHS_9 and 4CL_13 had higher expression levels in immature fruits (imSC and imPC) than in mature fruits (mSC and mPC) (Fig. 4C; Table S17). These findings suggested that the anthocyanin accumulation rate may be greater in immature fruits than in mature fruits, which was consistent with the findings of previous studies [48,49]. Furthermore, ANS_1, F3’5’H_7, F3H_2, CHS_9 and 4CL_13 generally had higher expression levels than the other anthocyanin synthesis-related genes in the bracts of Mo and Mv (Fig. 4C; Table S17), suggesting that these five genes may play important roles in bract coloration. In addition, these five structural genes showed higher expression levels in

imPC of Mv than in imPC of *Musa* spp. AAA (Fig. 4C; Table S17).

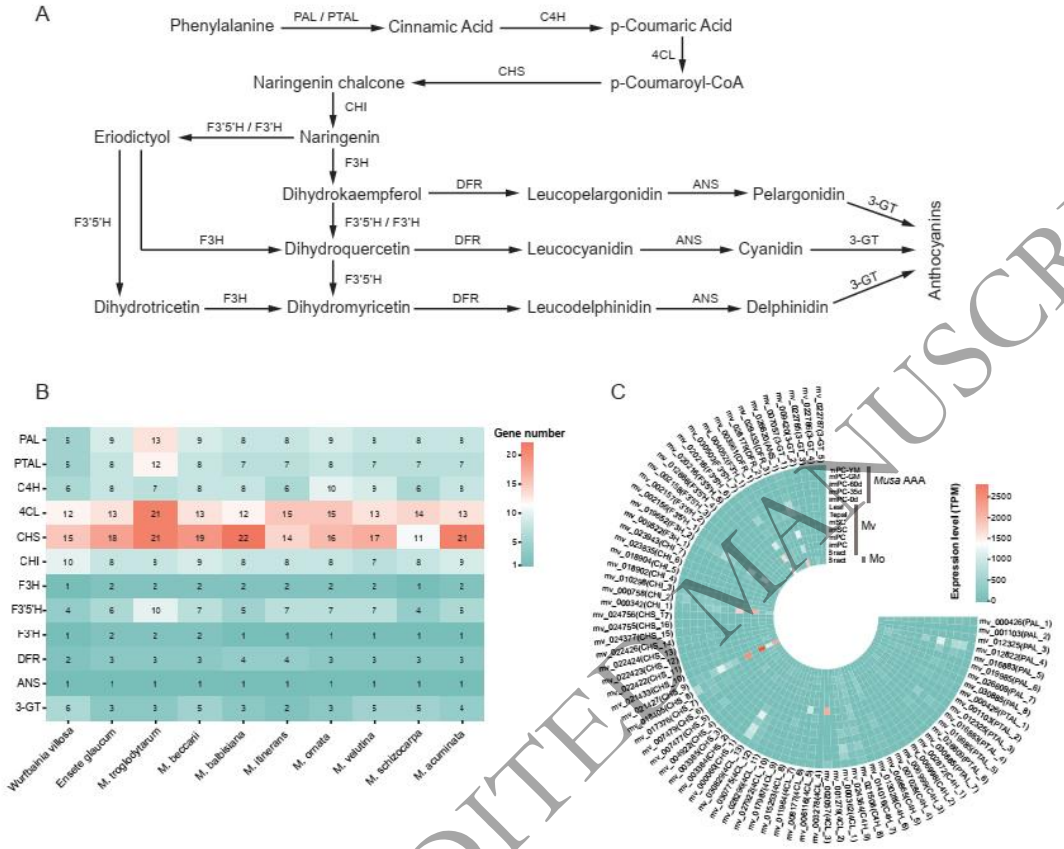

Figure 4 A: Anthocyanin biosynthesis pathway. PAL, phenylalanine ammonia-lyase; PTAL, phenylalanine/tyrosine ammonia-lyase; C4H, cinnamic 4-hydroxylase; 4CL, 4-coumarate CoA ligase; CHS, chalcone synthase; CHI, chalcone isomerase; F3H, flavanone 3-hydroxylase; F3'H, flavonoid 3'-hydroxylase; F3'5'H, flavonoid 3',5'-hydroxylase; DFR, dihydroflavonol 4-reductase; ANS, anthocyanidin synthase; 3-GT, anthocyanidin 3-O-glucosyltransferase. **B:** The number of enzyme-coding genes in anthocyanin biosynthesis pathway of 10 species. The number in each cell indicates gene number. **C:** Expression levels of enzyme-coding genes in the bracts of *M. ornata* and *M. velutina*. The expression values were standardized by the TPM method.

Discussion

Although Mo and Mv are widely cultivated as important ornamental plants in tropical regions [24], their genomes are still lacking, which hampers the plant molecular breeding efforts aimed at enhancing desirable traits. In this study, we generated

chromosome-level genomes for them. Both Mo and Mv were assembled into 11 pseudochromosomes with genome sizes of 427.85 Mb and 478.10 Mb, respectively. The contig N50, BUSCO assessment, mapping rate and LAI showed that the two genome assemblies had high continuity and completeness. Furthermore, we inferred the phylogenetic relationships and gene family expansion and contraction. DEGs in immature and mature pericarps were identified and the results showed that the significantly upregulated DEGs in mature pericarps were related primarily to saccharide metabolic processes at the cell wall or in the extracellular region. We compared the expression levels of PGs in different tissues and found that several PG genes had exceptionally high expression level in the mature pericarps. Additionally, we identified genes involved in the anthocyanin biosynthesis pathway in Mo and Mv.

Species relationships and divergence times are among the most crucial concerns for evolutionary biologists. According to our results, Mo and Mv were sister species and were closely related to *M. acuminata* and *M. schizocarpa*, followed by *M. itinerans* and *M. balbisiana*, which is largely in agreement with the findings of previous studies [18,23]. However, conflicting phylogenetic positions were previously observed for *M. schizocarpa* and *M. itinerans* based on nuclear and plastid loci [1,23,50], which may suggest a complex evolutionary history within *Musa*. The Musaceae crown age (split of *Ensete* and *Musa*) was estimated to be 51.9 Mya in our study, which is largely consistent with Fu et al. [23] (59.19 Mya). However, the Musaceae crown age estimated by Zhou et al. [18] was much younger at 9.89 Mya. Because the fossil *Ensete oregonense* was recovered from the middle Eocene of western North America (43 Mya) [51], the crown age Musaceae should not be less than 43 Mya. The divergence time estimated by Zhou et al. [18] might be biased due to the fossils or second calibration points used.

D'Hont et al. [14] indicated that the *Musa* lineage had experienced three rounds of WGD events. In this study, we observed two typical ones at ~0.55 and ~0.9 of Ks (Fig. S11), of which the peak at 0.55 likely represent the α and β WGD events around the Cretaceous-Paleocene boundary, and the peak at 0.9 indicates the more ancient γ

WGD event at approximately 100 Mya according to D'Hont et al. [14]. In addition, our results suggested that *Musa* species had no species-specific WGD events, which is congruent with the findings of previous studies [16,52]. In terms of structural variation between homologous chromosomes, no inversions or rearrangements have been detected in chr04 between *M. acuminata* and *M. balbisiana* [16]. This suggests that the variations in chr04 of Mo likely emerged after its divergence from Mv. Conversely, there are no structural variations among chr05 of *M. balbisiana*, chr05 of Mo, and chr03 of Mv. This indicates that the inversions observed in chr05 of *M. acuminata* and *M. schizocarpa* probably occurred after their divergence from Mo and Mv. Genome size variations in angiosperms are determined primarily by LTRs rather than by WGD, since LTRs occupy most of the genome content [53]. According to our results, the LTR length of Mv was ~204 Mb, greater than that of Mo (~166 Mb) and *M. acuminata* (~190 Mb) (Table S5), which could explain most of the variation among the three genomes. As ancient LTRs are prone to be recognized and eliminated [54,55], Mv (with generally older insertion times) should contain less LTRs than Mo does, which is contrary to our results but could be explained by the recent second peak at 0.5 Mya. Ancient LTRs can be eliminated by imbalanced homologous recombination and double-strand breaks [56]; thus, the lack of this removal mechanism may lead to the retainment of older LTRs in the Mv genome, which requires further investigation.

Pericarp dehiscence can facilitate seed dispersal in wild plants but result in yield loss in food crops. Although pericarp dehiscence has relatively limited impact on the value of ornamental plants, exploring its molecular mechanism could help biologists understand how this trait evolves among diverse plant groups and how it facilitates species adaptation to environment. The PG genes were shown to be essential for the development, ripening and abscission of fig fruits [45], as well as for the pod dehiscence of *Brassica napus* [57] and *Arabidopsis thaliana* [35]. In this study, we found that several PG genes (particularly MvPG11) had higher expression levels in mature pericarps and were likely responsible for the dehiscence of Mv fruits. In

contrast, no PG or CEL genes were highly expressed in the mature pericarps of *Musa* spp. AAA. According to our findings, MvPG11 was present in the Musaceae and Zingiberaceae, had quite similar amino acid sequences among different species and was under purifying or negative selection. Previous study revealed that genes under strong purifying or negative selection are functionally conserved [58]; therefore, MvPG11 may have a conserved gene function, and the dehiscence of Mv and indehiscence of other *Musa* species may be determined by the gene expression levels. Previous studies have indicated that the expression of PG genes is positively regulated by several transcription factors, such as AP2/ERF, the NAC and the MADS-box family transcription factors [45-47]. In this study, we identified potential TFBSs for PG genes and highly expressed TFs in mature pericarps; however, further experimental verification is needed. In addition, pericarp dehiscence has also been reported in the other *Musa* species, such as *M. schizocarpa* and some cultivars of *M. acuminata* [4,38]. These samples should also be included in the future to explore whether the same PG genes determines pericarp dehiscence in different species and how they are regulated by TFs.

Anthocyanins are natural pigments responsible for the purple, blue and red color in leaves, stems, flowers, fruits and roots of plants [59]. For example, the leaves and pseudostems of *Musa* spp. AAA changed from green to purple during its development stages, but remained green when the anthocyanin synthesis-related genes (e.g., CHS, ANS and DFR) were repressed by a MYB transcription factor [60], indicating that plant tissue colors may be determined by the expression of the anthocyanin synthesis-related genes. This study found that the expression levels of CHS_9, CHI_1, F3H_2, F3'5'H_7 and ANS_1 in the imPC of Mv were 2.56, 6.95, 1.36, 2.92 and 1.20 times more than those in imPC-0d of *Musa* spp. AAA (Fig. 4C; Table S17). The pericarp of Mv is pink during its development stages, while the pericarp of *Musa* spp. AAA is green and turns yellow-green when mature. This suggested that the differential expression of these structural genes might have led to the distinct peel colors of Mv and *Musa* spp. AAA. However, further research is needed to explore how these genes

508 determine color formation in banana tissues.

509 ## Materials and methods

510 ### Plant material collection and sequencing

511 Fresh and young leaves of Mo and Mv were collected from the South China Botanical
512 Garden (Guangdong, China) and subjected to genomic DNA extraction following the
513 procedures of the Qiagen Genomic DNA Kit. Degradation of the extracted DNA was
514 assessed by 0.75% gel electrophoresis; DNA purity was evaluated using a NanoDrop
515 One UV-Vis spectrophotometer (Thermo Fisher Scientific, USA); and DNA
516 concentration was measured utilizing Qubit 3.0 fluorometers (Thermo Fisher
517 Scientific, USA). High-quality DNA was used to prepare short and long read whole-
518 genome sequencing (WGS) libraries.

519 Total RNA was extracted using the TRNzol Universal RNA Extraction Kit (Tiangen,
520 Beijing, China). RNA of Mo was extracted from leaves, tepals and bracts. RNA of Mv
521 was extracted from leaves, tepals and bracts, as well as pericarps and sarcocarps at
522 immature and mature stages.

523 A paired-end (2 × 150 bp) Illumina library was prepared using the TruSeq Nano DNA
524 HT Sample Preparation Kit and subsequently sequenced using the Illumina HiSeq X
525 Ten platform (Illumina, San Diego, CA, USA). The Nanopore library was constructed
526 using the LSK109 Ligation Sequencing Kit (Oxford Nanopore Technologies, Oxford,
527 UK), and sequencing was performed using a Nanopore PromethION sequencer
528 (Oxford Nanopore Technologies, UK) at GrandOmics Co., Ltd. (Wuhan, China). The
529 Hi-C library was generated based on the method detailed in Belton et al. [61] with
530 some modifications. Briefly, young and fresh leaves were fixed in nuclei isolation
531 buffer with 2% formaldehyde. The cross-linked DNA was subsequently digested with
532 100 units of DpnII (New England Biolabs, USA). The digested fragments were
533 biotinylated with biotin-14-dCTP and ligated using T4 DNA polymerase (New
534 England Biolabs). The ligated DNA was enriched, sheared into 300- to 600-bp
535 fragments, blunt-end repaired, and further processed. The final paired-end (2 × 150

bp) Hi-C library was sequenced on the Illumina HiSeq X Ten platform. The RNA library was constructed using the TruSeq RNA Library Preparation Kit, and RNA sequencing was carried out on the Illumina HiSeq X Ten platform with paired-end reads (2 × 150 bp).

After sequencing, fastp v0.23.3 [62] was used to remove adapters and low-quality reads with default parameters from Illumina, Hi-C and RNA reads. Porechop v0.2.4 [63] was used to remove adapters from the Nanopore long reads.

K-mer analysis and genome assembly

Genome size was estimated using Illumina reads via Jellyfish v2.3.0 [64] and GenomeScope v1.0 [65] with a k-mer length of 21. Nanopore reads were used to assemble the genome via NextDenovo v2.5.1 [66]. Purge Haplotigs v1.1.2 [67] was utilized to identify and remove haplotypic duplications in the primary genome assemblies. Thereafter, the genome assemblies were polished using two rounds of Racon v1.5.0 [68] for Nanopore reads and hapo-G v1.3.4 [69] for Illumina reads. The polished genome assemblies were scaffolded with Hi-C reads using Juicer v1.6 [70] and 3d-dna v180922 [71] and then manually adjusted in Juicebox v1.11.08 [72]. Gaps in the genomes were filled with Nanopore reads using TGS-GapCloser v1.1.1 [73]. The gap-closed genome assemblies were further polished using Racon and hapo-G, respectively, each with two rounds. Gaps, telomeres and centromeres were subsequently identified using quarTeT v1.1.5 [74].

Genomic evaluation and repeat annotation

The integrity of the assembled genomes was assessed using BUSCO v5.3.2 [75] with the embryophyta_odb10.2020-09-10 database. To determine genome completeness, mapping rates were calculated by mapping Illumina reads to the genomes with BWA-MEM v0.7.17-r1188 [76] and RNA reads to genomes with HISAT2 v2.2.1 [77]. The percentage of mapped reads was subsequently determined with the “stats” command in BamTools v2.5.1 [78]. Genome assembly quality was evaluated by LTR assembly index (LAI), which was calculated by using the LAI program [79]. A Hi-C interaction

heatmap was generated using HiCExplorer v3 [80]. Repetitive sequence annotation was performed using the Extensive de novo TE Annotator (EDTA) v2.1.0 [81].

Gene structure and function annotation

Genomes were masked using RepeatModeler v2.0.1 [82] and RepeatMasker v4.1.2 [83]. Gene prediction and functional annotation were performed on the soft-masked genomes using funannotate v1.8.15 [84]. Briefly, the gene prediction models were trained via the "funannotate train" function based on the RNA reads. The protein-coding genes of Mo and Mv were predicted using the "funannotate predict" function, which employs GeneMark-ET v3.10-5 [85], Augustus v3.5.0 [86], SNAP v2013-02-16 [87] and GlimmerHMM v3.0.1 [88]. Additionally, the tRNAs were predicted by means of tRNAscan-SE v2.0.11 [89]. In this step, protein-coding sequences of *Ensete glaucum*, *M. acuminata*, *M. balbisiana*, *M. itinerans* and *M. schizocarpa* were downloaded from the Banana Genome Hub [90] as protein evidence (Table S4). Thereafter, the gene models were revised using the "funannotate update" feature. InterProScan v5.62-94.0 [91] and the local version of EggNOG-mapper v2.1.11 [92] were used to identify motifs and protein domains by matching against public databases. The results of the InterProScan and EggNOG-mapper analyses were merged using the "funannotate annotate" feature.

Gene family expansion, contraction, and GO enrichment analysis

Gene orthologs and gene duplication events of Mo and Mv were identified using OrthoFinder v2.5.4 [93] by comparison with eight other species in the Musaceae and Zingiberaceae (Table S6). Based on the species tree inferred by OrthoFinder, divergence time was estimated using a penalized-likelihood method implemented in treePL v1.0 [94]. The crown age of the Zingiberales was calibrated to 83.5 million years ago (Mya) using *Spirematospermum chandlerae* [95], the oldest-known fossil of the order. The crown age of Musaceae estimated by Janssens et al. [50] (51.9 Mya) was used to constrain the split of *Ensete*/*Musa*. Gene family expansions or contractions were detected using CAFE v5.0 [96]. GO enrichment analysis was

performed for unique gene families, as well as significantly expanded and contracted gene families using the enricher function in the R package clusterProfiler v4.8.2 [97].

Genome synteny, duplications and whole-genome comparisons

Genome synteny analysis was performed based on the genomes of Mo, Mv and *M. acuminata*. The orthologs were identified and filtered with the parameters --cscore=.99 and --minspan=30, and the final synteny plot was visualized using the MCscan pipeline [98] following Huang et al. [17]. Hi-C signals surrounding large inversions and translocations were visualized using HiCExplorer v3. Duplicated gene pairs of Mo and Mv were classified into WGD, TD, PD, TRD and DD using the R package doubletrouble v1.0.0 [99]. *M. acuminata* was set as an outgroup in the analysis. The program WGDI v0.6.5 [100] was used to infer the polyploidization events in *M. acuminata*, Mo and Mv. Collinear genes were identified using the "-icl" option of WGDI within each genome, and Ks were calculated using the "-ks" option with the Nei-Gojobori method implemented in the YN00 program in PAML v4.9h [101]. The Gaussian fitting curve parameters of each Ks peak were used to produce the Ks distribution map with the "-kf" option. To model the changes in effective population size through time, the program PSMC v0.6.5-r67 [102] was used to infer the population history of Mo, Mv and *M. acuminata* based on individual whole-genome sequences. The Illumina reads of *M. acuminata* used in this analysis were downloaded from the European Nucleotide Archive under project PRJEB35002 (Table S6). Ka/Ks were calculated for the genes of Mo and Mv using TBtools v1.120 [103] with the Nei-Gojobori model. Positively selected genes were subjected to GO enrichment analysis using the R package clusterProfiler.

Differentially expressed gene analysis of Mv

In the present study, the dehiscent pericarp indicates the maturity of Mv fruits. RNA of Mv was sequenced for immature pericarps (imPC) and sarcocarps (imSC), as well as mature pericarps (mPC) and sarcocarps (mSC). The reads for gene exons were counted using featureCounts v2.0.6 [104]. DEGs were identified using the DEGexp

function with the MARS method in the R package DEGseq v1.54.0 [105]. The DEGs between imPC and mPC as well as between imSC and mSC were selected with the criterion of absolute normalized log_2-transformed fold-change > 2 and p-value < 0.001. GO enrichment analysis of the upregulated DEGs was performed using the enricher function in the R package clusterProfiler.

Identification of pericarp dehiscence-related genes in Mv

Based on the Hidden Markov Model (HMM) file of the polygalacturonase (PG) protein domain PF00295 from the Pfam database (https://www.ebi.ac.uk/interpro/), the PG genes were searched for within the protein sequences using HMMER v3.3.2 [44] (e-value ≤ 1e-5). Five protein sequences (Table S18) of the cellulase (CEL) family genes from *Arabidopsis thaliana* and *Glycine max* were downloaded from the National Center for Biotechnology Information (NCBI) and aligned using MAFFT v7.508 [106]. The alignments were used to generate the HMM file, and the CEL genes were searched for within the protein sequences using HMMER (e-value ≤ 1e-5). Protein sequences without conserved domains or motifs were excluded. The remaining sequences were subsequently aligned using MAFFT, and sites with more than 50% gaps were removed using ClipKIT [107]. The alignment was used to construct a maximum likelihood tree in IQ-TREE v1.6.12 with 1000 ultrafast bootstraps [108]. The best-fit model (JTT+R6) was determined by ModelFinder [109] according to the BIC criterion. Nonsynonymous substitution rates (Ka), Ks and Ka/Ks were calculated using the Nei-Gojobori model in TBtools. The chromosomal location of the PG genes was illustrated with TBtools. Potential TFBSs in the promoter sequences of the PG genes were predicted using the online program JASPAR (https://jaspar.elixir.no/) with relative profile score threshold > 90% [110]. Upstream 2000 bp sequences of the PG genes were extracted for the analysis.

The AP2/ERF, NAC and MADS-box transcription factors have been shown to upregulate the expression of PG genes that are related to fruit ripening and softening [45,47,111]. To explore whether these transcription factors had high expression levels in the mature pericarps, we downloaded the HMM files of AP2/ERF (PF00847), NAC

649 (PF01849 and PF02365) and MADS-box (SRF domain PF00319 and MEF2 domain
650 PF09047) from the Pfam database and searched the transcription factors using
651 HMMER (e-value ≤ 1e-5). Besides, we downloaded the protein sequences of
652 AP2/ERF, NAC and MADS-box of *Musa acuminata* from the PlantTFDB
653 (http://planttfdb.gao-lab.org/), and searched for the transcription factors using blastp
654 v2.11.0 [112] with e-value ≤ 1e-5, score ≥ 100 and coverage ≥ 80. The results of
655 HMMER and blastp were combined, repeated transcription factors were removed, and
656 conserved domains and motifs were checked.

657 To investigate whether the identified genes were highly expressed in mature but
658 indehiscent pericarps, RNA from various stages of the pericarps of dwarf banana
659 (*Musa* spp. AAA) [113] was obtained from the National Genomics Data Center
660 (NGDC), China National Center for Bioinformation (CNCB) (Table S6). Read counts
661 were standardized in R v4.3.1 [114] with the TPM method, which accounts for the
662 effects of sequencing depth and gene length among different samples. A heatmap
663 displaying gene expression levels was generated with TBtools and ChiPlot
664 (https://www.chiplot.online/). The microsynteny of the highly expressed PG genes
665 and adjacent regions across multiple species was visualized using the MCscan
666 pipeline.

667 **Anthocyanin biosynthesis pathway**

668 The anthocyanin biosynthesis pathway was obtained from the KEGG PATHWAY
669 Database (https://www.kegg.jp/kegg/pathway.html). Protein sequences were
670 functionally annotated using EggNOG-mapper. Genes encoding enzymes in the
671 pathway were extracted from the annotations. RNA reads of Mo, Mv and *Musa* spp.
672 AAA were mapped to the Mv genome, and read counts were standardized using the
673 TPM method. The gene number and expression level heatmaps were visualized using
674 ChiPlot.

675

676

Acknowledgments

This work was financially supported by the National Natural Science Foundation of China (No. 32070237, 31261140366). We thank Yu-Ying Zhou of South China Botany Garden CAS for her help in material freezing and Xiao-Xia Zhang from Institute of Botany CAS for her suggestions on gene family analysis.

Author contributions

X.J.G. and H.R.H conceived the project. X.J.G. and T.W.X. collected the materials. T.W.X., X.L., N.F., T.J.L. and Z.F.W. performed the analyses. T.W.X. wrote the manuscript. X.J.G., H.R.H. and Z.F.W revised the manuscript. All authors approved the final manuscript.

Data availability

All the raw sequence data were deposited in the Genome Sequence Archive in the National Genomics Data Center (NGDC), China National Center for Bioinformation (CNCB) with the accession number of CRA013014 under BioProject PRJCA020485 (https://ngdc.cncb.ac.cn/). The genome assemblies reported in this study were deposited in the Genome Warehouse in NGDC, CNCB under the accession number GWHDVGC00000000 (*Musa ornata*) and GWHDVGD00000000 (*Musa velutina*). In addition, the genome assemblies, protein-coding sequences, as well as genome annotations were deposited in the Science Data Bank [115] and figshare [116].

Conflict of interest

The authors declare that they have no competing interests.

Supplementary Data

Figure S1 Genome survey of *M. ornata* and *M. velutina*.

Figure S2 Locations of centromeres, telomeres and gaps in the genomes.

Figure S3 BUSCO assessment of genome assemblies.

Figure S4 Hi-C interaction heatmaps of Mo (A) and Mv (B) (bin size 10,000 bp).

Figure S5 BUSCO assessment of protein sequences.

Figure S6 GO enrichment of unique gene families of *M. ornata* (A) and *M. velutina* (B).

Figure S7 Divergence time of Musaceae.

Figure S8 GO enrichment of the significantly expanded gene families in *M. ornata* (A) and *M. velutina* (B), and significantly contracted gene families in *M. ornata* (C) and *M. velutina* (D).

Figure S9 Hi-C signals surrounding the inversions and translocations. Block IDs were named according to their positions on chromosome 4 of *M. ornata*. Block ranges were marked above each plot.

Figure S10 The number of gene pairs and unique genes for each gene duplication type (DD, PD, TD, TRD and WGD).

Figure S11 Distribution of synonymous nucleotide substitutions (Ks). Collinear gene blocks were identified by comparing the proteins of *M. ornata* to *M. ornata*, *M. velutina* to *M. velutina* and *M. acuminata* to *M. acuminata*.

Figure S12 Ka/Ks distribution patterns of *M. ornata* and *M. velutina*. *M. acuminata* was used as reference.

Figure S13 GO enrichment of positively selected genes of *M. ornata* (A) and *M. velutina* (B).

Figure S14 Historical effective population sizes of *M. ornata*, *M. velutina* and *M. acuminata*.

Figure S15 GO enrichment of downregulated genes in mature pericarps (A) and mature sarcocarps (B).

Figure S16 Protein sequence alignments of the PG family genes. Only a subset of PG genes is shown for presentation convenience. Four domains (i.e., SPNDG, GDDC, PGHG and RIK) are marked. The background of the amino acid that was uniquely present in MvPG11/mv_006393 (i.e., methionine at position 351 of the alignment) is red.

Figure S17 Maximum likelihood tree of the PG genes. The red clade includes all

orthologs of MvPG11/mv_006393.

Figure S18 The expression levels of AP2/ERF, NAC and MADS-box. Only transcript factors that were upregulated in mature pericarps are shown.

Table S1 Summary of the Illumina reads, Hi-C reads, Nanopore reads and RNA-seq reads.

Table S2 Sequence length and gap number for each pseudochromosome.

Table S3 Location, number and direction of the telomeric repeats.

Table S4 Summary of the centromeric regions.

Table S5 Summary of the repetitive sequences inferred by EDTA.

Table S6 The downloaded genomes, Illumina reads and RNA-seq reads.

Table S7 Summary of functional annotations of *M. ornata* and *M. velutina*.

Table S8 Significantly expanded and contracted gene families of *M. ornata* and *M. velutina*.

Table S9 Gene list for each gene duplication type (DD, PD, TD, TRD and WGD).

Table S10 Differentially expressed genes in *M. velutina* pericarps.

Table S11 Differentially expressed genes in *M. velutina* sarcocarps.

Table S12 GO enrichment of upregulated genes in mature pericarps of *M. velutina*.

Table S13 GO enrichment of upregulated genes in mature sarcocarps of *M. velutina*.

Table S14 The expression levels of the PG and CEL genes.

Table S15 Ka, Ks and Ka/Ks of the PG genes.

Table S16 Potential transcript factor binding sites predicted by JASPAR.

Table S17 Expression levels of the genes involved in the anthocyanin biosynthesis pathway in different tissues and species.

Table S18 Accession numbers of the CEL genes from *Arabidopsis thaliana* and *Glycine max*.

Reference:

1. Burgos-Hernández M, Pozo C, González D. Evolutionary history of Musaceae: ancient distribution and the rise of modern lineages. *Bot J Linn Soc*. 2018;189:23-35.
2. Heslop-Harrison JS, Schwarzacher T. Domestication, genomics and the future for banana. *Ann Bot*. 2007;100:1073–1084.
3. Sardos J, Breton C, Perrier X et al. Hybridization, missing wild ancestors and the domestication of cultivated diploid bananas. *Front Plant Sci*. 2022;13:969220.
4. Häkkinen M. Ornamental bananas: focus on *Rhodochlamys*. *Chron Hortic*. 2007;47:7–12.
5. Joe A, Sabu M. Wild ornamental bananas in India: an overview. *South Indian J Biol Sci*. 2016;2:213–221.
6. Krug AS, B. M. Drummond E, Van Tassel DL et al. The next era of crop domestication starts now. *Proc Natl Acad Sci USA*. 2023;120:e2205769120.
7. Gui S, Martinez-Rivas FJ, Wen W et al. Going broad and deep: sequencing-driven insights into plant physiology, evolution, and crop domestication. *Plant J*. 2023;113:446–459.
8. Sun M, Yao C, Shu Q et al. Telomere-to-telomere pear (*Pyrus pyrifolia*) reference genome reveals segmental and whole genome duplication driving genome evolution. *Hortic Res*. 2023;10:uhad201.
9. Li P, Bai G, He J et al. Chromosome-level genome assembly of *Amomum tsao-ko* provides insights into the biosynthesis of flavor compounds. *Hortic Res*. 2022;9:uhac211.
10. Wang X, Gao Y, Wu X et al. High-quality evergreen azalea genome reveals tandem duplication-facilitated low-altitude adaptability and floral scent evolution. *Plant Biotechnol J*. 2021;19:2544–2560.
11. Liao X, Ye Y, Zhang X et al. The genomic and bulked segregant analysis of *Curcuma alismatifolia* revealed its diverse bract pigmentation. *aBIOTECH*. 2022;3:178–196.
12. Lan L, Zhao H, Xu S et al. A high-quality *Bougainvillea* genome provides new insights into evolutionary history and pigment biosynthetic pathways in the Caryophyllales. *Hortic Res*. 2023;10:uhad124.
13. He S, Weng D, Zhang Y et al. A telomere-to-telomere reference genome provides genetic insight into the pentacyclic triterpenoid biosynthesis in *Chaenomeles speciosa*. *Hortic Res*. 2023;10:uhad183.
14. D'Hont A, Denoeud F, Aury J-M et al. The banana (*Musa acuminata*) genome and the evolution of monocotyledonous plants. *Nature*. 2012;488:213–217.
15. Belser C, Baurens F-C, Noel B et al. Telomere-to-telomere gapless chromosomes of banana using nanopore sequencing. *Commun Biol*. 2021;4:1047.
16. Wang Z-F, Rouard M, Droc G et al. Genome assembly of *Musa beccarii* shows extensive chromosomal rearrangements and genome expansion during evolution of Musaceae genomes. *GigaScience*. 2023;12:giad005.
17. Huang H-R, Liu X, Arshad R et al. Telomere-to-telomere haplotype-resolved reference genome reveals subgenome divergence and disease resistance in triploid Cavendish banana. *Hortic Res*. 2023;10:uhad153.
18. Zhou R, Wang S, Zhan N et al. High-quality reference genome assemblies for two *Australimusa* bananas provide insights into genetic diversity of the Musaceae family and regulatory mechanisms of superior fiber properties. *Plant Commun*. 2023;5:100681.

19. Li Z, Wang J, Fu Y et al. The *Musa troglodytarum* L. genome provides insights into the mechanism of non-climacteric behaviour and enrichment of carotenoids. *BMC Biol*. 2022;20:186.
20. Rouard M, Droc G, Martin G et al. Three new genome assemblies support a rapid radiation in *Musa acuminata* (wild banana). *Genome Biol Evol*. 2018;10:3129–3140.
21. Wang Z, Miao H, Liu J et al. *Musa balbisiana* genome reveals subgenome evolution and functional divergence. *Nature Plants*. 2019;5:810–821.
22. Li X, Yu S, Cheng Z et al. Origin and evolution of the triploid cultivated banana genome. *Nat Genet*. 2024;56:136–142.
23. Fu N, Ji M, Rouard M et al. Comparative plastome analysis of Musaceae and new insights into phylogenetic relationships. *BMC Genomics*. 2022;23:223.
24. Sachter-Smith G. The Wild Bananas: a catalogue of wild *Musa* species and tribute to Markku Häkkinen. Bioversity International, 2023.
25. Shankar K, Haokip SW, Ramjan M et al. Genetic diversity of fruits in North East region of India. *J Pharmacogn Phytochem*. 2020;9:207–209.
26. Onstein RE, Kissling WD, Chatrou LW et al. Which frugivory-related traits facilitated historical long-distance dispersal in the custard apple family (Annonaceae)? *J Biogeogr*. 2019;46:1874–1888.
27. Pansarin ER, Suetsugu K. Mammal-mediated seed dispersal in *Vanilla*: Its rewards and clues to the evolution of fleshy fruits in orchids. *Ecology*. 2022;103:e3701.
28. Christiansen LC, Dal Degan F, Ulvskov P et al. Examination of the dehiscence zone in soybean pods and isolation of a dehiscence-related endopolygalacturonase gene. *Plant, Cell Environ*. 2002;25:479–490.
29. Zamil MS, Geitmann A. The middle lamella—more than a glue. *Physical Biology*. 2017;14:015004.
30. Abbott DW, Boraston AB. The structural basis for exopolygalacturonase activity in a family 28 Glycoside Hydrolase. *J Mol Biol*. 2007;368:1215–1222.
31. Li Q, Wu Z, Wu H et al. Transcriptome profiling unravels a vital role of pectin and pectinase in anther dehiscence in *Chrysanthemum*. *Int J Mol Sci*. 2019;20:5865.
32. Chen J, Duan Y, Hu Y et al. Transcriptome analysis of atemoya pericarp elucidates the role of polysaccharide metabolism in fruit ripening and cracking after harvest. *BMC Plant Biol*. 2019;19:219.
33. Kalaitzis P, Solomos T, Tucker ML. Three different polygalacturonases are expressed in tomato leaf and flower abscission, each with a different temporal expression pattern. *Plant Physiol*. 1997;113:1303–1308.
34. Taylor JE, Webb STJ, Coupe SA et al. Changes in polygalacturonase activity and solubility of polyuronides during ethylene-stimulated leaf abscission in *Sambucus nigra*. *J Exp Bot*. 1993;44:93–98.
35. Ogawa M, Kay P, Wilson S et al. ARABIDOPSIS DEHISCENCE ZONE POLYGALACTURONASE1 (ADPG1), ADPG2, and QUARTET2 are polygalacturonases required for cell separation during reproductive development in *Arabidopsis*. *The Plant Cell*. 2009;21:216–233.
36. Heredia A, Jiménez A, Guillén R. Composition of plant cell walls. *Zeitschrift für Lebensmittel-Untersuchung und Forschung*. 1995;200:24–31.

37. Merelo P, Agusti J, Arbona V et al. Cell wall remodeling in abscission zone cells during ethylene-promoted fruit abscission in *Citrus*. *Front Plant Sci*. 2017;8:126.
38. Ploetz RC, Kepler AK, Daniells J et al. Banana and plantain—an overview with emphasis on Pacific island cultivars. *Species Profiles for Pacific Island Agroforestry*. 2007;1:21–32.
39. Landi M, Tattini M, Gould KS. Multiple functional roles of anthocyanins in plant-environment interactions. *Environ Exp Bot*. 2015;119:4–17.
40. Winkel-Shirley B. Flavonoid biosynthesis. A colorful model for genetics, biochemistry, cell biology, and biotechnology. *Plant Physiol*. 2001;126:485–493.
41. Mol J, Grotewold E, Koes R. How genes paint flowers and seeds. *Trends Plant Sci*. 1998;3:212–217.
42. Deng S, Cheng C, Liu Z et al. Comparative transcriptome analysis reveals a role for anthocyanin biosynthesis genes in the formation of purple peel in Minhou wild banana (*Musa itinerans* Cheesman). *J Hortic Sci Biotechnol*. 2019;94:184–200.
43. Fu X, Cheng S, Liao Y et al. Comparative analysis of pigments in red and yellow banana fruit. *Food Chem*. 2018;239:1009–1018.
44. Eddy SR. Accelerated profile HMM searches. *PLoS Comp Biol*. 2011;7:e1002195.
45. Wang Y, Fan Z, Zhai Y et al. Polygalacturonase gene family analysis identifies *FcPG12* as a key player in fig (*Ficus carica* L.) fruit softening. *BMC Plant Biol*. 2023;23:320.
46. Nakano T, Kato H, Shima Y et al. Apple SVP Family MADS-Box proteins and the tomato pedicel abscission zone regulator JOINTLESS have similar molecular activities. *Plant Cell Physiol*. 2015;56:1097–1106.
47. Qi X, Dong Y, Liu C et al. The *PavNAC56* transcription factor positively regulates fruit ripening and softening in sweet cherry (*Prunus avium*). *Physiol Plant*. 2022;174:e13834.
48. Wu M, Liu J, Song L et al. Differences among the anthocyanin accumulation patterns and related gene expression levels in red pears. *Plants (Basel)*. 2019;8:100.
49. Pandey A, Alok A, Lakhwani D et al. Genome-wide expression analysis and metabolite profiling elucidate transcriptional regulation of flavonoid biosynthesis and modulation under abiotic stresses in banana. *Sci Rep*. 2016;6:31361.
50. Janssens SB, Vandelook F, De Langhe E et al. Evolutionary dynamics and biogeography of Musaceae reveal a correlation between the diversification of the banana family and the geological and climatic history of Southeast Asia. *New Phytol*. 2016;210:1453–1465.
51. Manchester SR, Kress WJ. Fossil bananas (Musaceae): *Ensete oregonense* sp. nov. from the Eocene of western North America and its phytogeographic significance. *Am J Bot*. 1993;80:1264–1272.
52. Wang Z, Rouard M, Biswas MK et al. A chromosome-level reference genome of *Ensete glaucum* gives insight into diversity and chromosomal and repetitive sequence evolution in the Musaceae. *GigaScience*. 2022;11:giac027.
53. Wang D, Zheng Z, Li Y et al. Which factors contribute most to genome size variation within angiosperms? *Ecol Evol*. 2021;11:2660–2668.
54. McCue AD, Nuthikattu S, Slotkin RK. Genome-wide identification of genes regulated in trans by transposable element small interfering RNAs. *RNA Biol*. 2013;10:1379–1395.
55. Oliver KR, McComb JA, Greene WK. Transposable elements: powerful contributors to angiosperm evolution and diversity. *Genome Biol Evol*. 2013;5:1886–1901.
56. Devos KM, Brown JKM, Bennetzen JL. Genome size reduction through illegitimate

recombination counteracts genome expansion in *Arabidopsis*. *Genome Res*. 2002;12:1075–1079.
57. Petersen M, Sander L, Child R et al. Isolation and characterisation of a pod dehiscence zone-specific polygalacturonase from *Brassica napus*. *Plant Mol Biol*. 1996;31:517–527.
58. Liu L, Wu Y, Liao Z et al. Evolutionary conservation and functional divergence of the LFK gene family play important roles in the photoperiodic flowering pathway of land plants. *Heredity*. 2018;120:310–328.
59. de Pascual-Teresa S, Sanchez-Ballesta MT. Anthocyanins: from plant to health. *Phytochem Rev*. 2008;7:281–299.
60. Deng G-M, Zhang S, Yang Q-S et al. *MaMYB4*, an R2R3-MYB repressor transcription factor, negatively regulates the biosynthesis of anthocyanin in banana. *Front Plant Sci*. 2021;11:600704.
61. Belton J-M, McCord RP, Gibcus JH et al. Hi–C: A comprehensive technique to capture the conformation of genomes. *Methods*. 2012;58:268–276.
62. Chen S, Zhou Y, Chen Y et al. fastp: an ultra-fast all-in-one FASTQ preprocessor. *Bioinformatics*. 2018;34:i884–i890.
63. Wick RR, Judd LM, Gorrie CL et al. Completing bacterial genome assemblies with multiplex MinION sequencing. *Microb Genom*. 2017;3:e000132.
64. Marçais G, Kingsford C. A fast, lock-free approach for efficient parallel counting of occurrences of k-mers. *Bioinformatics*. 2011;27:764–770.
65. Vurture GW, Sedlazeck FJ, Nattestad M et al. GenomeScope: fast reference-free genome profiling from short reads. *Bioinformatics*. 2017;33:2202–2204.
66. Jiang H, Zhuo W, Zongyi S et al. An efficient error correction and accurate assembly tool for noisy long reads. *bioRxiv*. 2023. doi:10.1101/2023.03.09.531669.
67. Roach MJ, Schmidt SA, Borneman AR. Purge Haplotigs: allelic contig reassignment for third-gen diploid genome assemblies. *BMC Bioinform*. 2018;19:460.
68. Vaser R, Sovic I, Nagarajan N et al. Fast and accurate de novo genome assembly from long uncorrected reads. *Genome Res*. 2017;27:737–746.
69. Aury J-M, Istace B. Hapo-G, haplotype-aware polishing of genome assemblies with accurate reads. *NAR Genom Bioinform*. 2021;3:lqab034.
70. Durand NC, Shamim MS, Machol I et al. Juicer provides a one-click system for analyzing loop-resolution Hi-C experiments. *Cell Syst*. 2016;3:95–98.
71. Dudchenko O, Batra SS, Omer AD et al. De novo assembly of the *Aedes aegypti* genome using Hi-C yields chromosome-length scaffolds. *Science*. 2017;356:92–95.
72. Durand NC, Robinson JT, Shamim MS et al. Juicebox provides a visualization system for Hi-C contact maps with unlimited zoom. *Cell Syst*. 2016;3:99–101.
73. Xu M, Guo L, Gu S et al. TGS-GapCloser: a fast and accurate gap closer for large genomes with low coverage of error-prone long reads. *GigaScience*. 2020;9:giaa094.
74. Lin Y, Ye C, Li X et al. quarTeT: a telomere-to-telomere toolkit for gap-free genome assembly and centromeric repeat identification. *Hortic Res*. 2023;10:uhad127.
75. Manni M, Berkeley MR, Seppey M et al. BUSCO update: novel and streamlined workflows along with broader and deeper phylogenetic coverage for scoring of eukaryotic, prokaryotic, and viral genomes. *Mol Biol Evol*. 2021;38:4647–4654.
76. Li H. Aligning sequence reads, clone sequences and assembly contigs with BWA-MEM.

arXiv. 2013;00:1–3.

77. Kim D, Paggi JM, Park C et al. Graph-based genome alignment and genotyping with HISAT2 and HISAT-genotype. *Nat Biotechnol*. 2019;37:907–915.

78. Barnett DW, Garrison EK, Quinlan AR et al. BamTools: a C++ API and toolkit for analyzing and managing BAM files. *Bioinformatics*. 2011;27:1691–1692.

79. Ou S, Chen J, Jiang N. Assessing genome assembly quality using the LTR Assembly Index (LAI). *Nucleic Acids Res*. 2018;46:e126–e126.

80. Wolff J, Rabbani L, Gilsbach R et al. Galaxy HiCExplorer 3: a web server for reproducible Hi-C, capture Hi-C and single-cell Hi-C data analysis, quality control and visualization. *Nucleic Acids Res*. 2020;48:W177–W184.

81. Ou S, Su W, Liao Y et al. Benchmarking transposable element annotation methods for creation of a streamlined, comprehensive pipeline. *Genome Biol*. 2019;20:275.

82. Flynn JM, Hubley R, Goubert C et al. RepeatModeler2 for automated genomic discovery of transposable element families. *Proc Natl Acad Sci USA*. 2020;117:9451–9457.

83. Tarailo-Graovac M, Chen N. Using RepeatMasker to identify repetitive elements in genomic sequences. *Curr Protoc Bioinformatics*. 2009;25:4.10.1–4.10.14.

84. Palmer JM, Stajich J. Funannotate v1.8.15: Eukaryotic genome annotation. *Zenodo*. 2020. https://zenodo.org/records/4054262.

85. Lomsadze A, Ter-Hovhannisyan V, Chernoff YO et al. Gene identification in novel eukaryotic genomes by self-training algorithm. *Nucleic Acids Res*. 2005;33:6494–6506.

86. Hoff KJ, Stanke M. Predicting genes in single genomes with AUGUSTUS. *Curr Protoc Bioinformatics*. 2019;65:e57.

87. Korf I. Gene finding in novel genomes. *BMC Bioinform*. 2004;5:59.

88. Majoros WH, Pertea M, Salzberg SL. TigrScan and GlimmerHMM: two open source ab initio eukaryotic gene-finders. *Bioinformatics*. 2004;20:2878–2879.

89. Lowe TM, Eddy SR. tRNAscan-SE: a program for improved detection of transfer RNA genes in genomic sequence. *Nucleic Acids Res*. 1997;25:955–964.

90. Droc G, Martin G, Guignon V et al. The banana genome hub: a community database for genomics in the Musaceae. *Hortic Res*. 2022;9:uhac221.

91. Jones P, Binns D, Chang H-Y et al. InterProScan 5: genome-scale protein function classification. *Bioinformatics*. 2014;30:1236–1240.

92. Huerta-Cepas J, Forslund K, Coelho LP et al. Fast genome-wide functional annotation through orthology assignment by eggNOG-Mapper. *Mol Biol Evol*. 2017;34:2115–2122.

93. Emms DM, Kelly S. OrthoFinder: phylogenetic orthology inference for comparative genomics. *Genome Biol*. 2019;20:238.

94. Smith SA, O'Meara BC. treePL: divergence time estimation using penalized likelihood for large phylogenies. *Bioinformatics*. 2012;28:2689–2690.

95. Friis EM. *Spirematosphermum chandlerae* sp. nov., an extinct species of Zingiberaceae from the North American Cretaceous. *Tertiary Research*. 1987;9:7–12.

96. Mendes FK, Vanderpool D, Fulton B et al. CAFE 5 models variation in evolutionary rates among gene families. *Bioinformatics*. 2020;36:5516–5518.

97. Wu T, Hu E, Xu S et al. clusterProfiler 4.0: a universal enrichment tool for interpreting omics data. *The Innovation*. 2021;2:100141.

98. Tang H, Bowers JE, Wang X et al. Synteny and collinearity in plant genomes. *Science*.

2008;320:486–488.
99. Almeida-Silva F, Van de Peer Y. doubletrouble: Identification and classification of duplicated genes. 2022. https://github.com/almeidasilvaf/doubletrouble.
100. Sun P, Jiao B, Yang Y et al. WGDI: a user-friendly toolkit for evolutionary analyses of whole-genome duplications and ancestral karyotypes. *Mol Plant*. 2022;15:1841–1851.
101. Yang Z. PAML 4: Phylogenetic analysis by maximum likelihood. *Mol Biol Evol*. 2007;24:1586–1591.
102. Li H, Durbin R. Inference of human population history from individual whole-genome sequences. *Nature*. 2011;475:493–496.
103. Chen C, Chen H, Zhang Y et al. TBtools: an integrative toolkit developed for interactive analyses of big biological data. *Mol Plant*. 2020;13:1194–1202.
104. Liao Y, Smyth GK, Shi W. featureCounts: an efficient general purpose program for assigning sequence reads to genomic features. *Bioinformatics*. 2013;30:923–930.
105. Wang L, Feng Z, Wang X et al. DEGseq: an R package for identifying differentially expressed genes from RNA-seq data. *Bioinformatics*. 2009;26:136–138.
106. Katoh K, Standley DM. MAFFT multiple sequence alignment software version 7: improvements in performance and usability. *Mol Biol Evol*. 2013;30:772–780.
107. Steenwyk JL, Buida TJ, III, Li Y et al. ClipKIT: a multiple sequence alignment trimming software for accurate phylogenomic inference. *PLoS Biol*. 2020;18:e3001007.
108. Nguyen L-T, Schmidt HA, von Haeseler A et al. IQ-TREE: a fast and effective stochastic algorithm for estimating maximum-likelihood phylogenies. *Mol Biol Evol*. 2014;32:268–274.
109. Kalyaanamoorthy S, Minh BQ, Wong TKF et al. ModelFinder: fast model selection for accurate phylogenetic estimates. *Nat Methods*. 2017;14:587–589.
110. Sandelin A, Alkema W, Engström P et al. JASPAR: an open-access database for eukaryotic transcription factor binding profiles. *Nucleic Acids Res*. 2004;32:D91–D94.
111. Qi X, Liu C, Song L et al. *PaMADS7*, a MADS-box transcription factor, regulates sweet cherry fruit ripening and softening. *Plant Sci*. 2020;301:110634.
112. Camacho C, Coulouris G, Avagyan V et al. BLAST+: architecture and applications. *BMC Bioinform*. 2009;10:421.
113. Ning T, Chen C, Yi G et al. Changes in homogalacturonan metabolism in banana peel during fruit development and ripening. *Int J Mol Sci*. 2022;23:243.
114. R Core Team. R: A language and environment for statistical computing. 2023. http://www.R-project.org/.
115. Xiao T-W, Wang Z-F, Ge X-J. Genome assembly of *Musa ornata* and *M. velutina*. 2023. https://doi.org/10.57760/sciencedb.12208.
116. Xiao T-W, Wang Z-F, Ge X-J. Genome sequences, proteins, cds, and annotation files of *Musa ornata* and *Musa velutina*. 2024. https://doi.org/10.6084/m9.figshare.25323370.v1.